Sixteen-Color Photometry of Galaxy Cluster Abell 566

Xu Zhou,[1,2] Nobuo Arimoto,[3,4] Ichi Tanaka,[4] Zhaoji Jiang,[1] Jiansheng Chen[1]

[1] *National Astronomical Observatories, Chinese Academy of Sciences, Beijing 100012, P.R.China*

[2] *The Institute for Physical and Chemical Research (RIKEN),2-1 Hirosawa, Wako, Saitama 351-0198*

[3] *Institute of Astronomy, School of Science, The University of Tokyo, Mitaka, Tokyo 181-0015*

[4] *National Astronomical Observatory, Mitaka, Tokyo 181-8588*

zhouxu@vega.bac.pku.edu.cn

(Received 2000 December 27; accepted 2003 July 30)

Abstract

We present a complete set of 16 color photometric observations in the Beijing–Arizona–Taipei–Connecticut (BATC) filter system for a cluster of galaxy Abell 566 at redshift $z \simeq 0.1$. From 2k $\times$ 2k CCD images, over 10000 objects have been detected in field of $58' \times 58'$ down to $V \sim 20$ mag with a good completeness level. By aperture photometric measurements, we obtained spectral energy distributions (SEDs) that cover the wavelengths from $300nm$ to $1000nm$ of all of the detected objects, including 561 cluster member candidates selected by the method of photometric redshift. The special location of these galaxies in color–color diagrams show a possibility for our method involving member galaxy selection. From the selected member galaxies, we find that the number density of early-type galaxies is much higher in the central region of the cluster than late-type galaxies.

Key words: galaxies:clusters:individual(Abell 566)—galaxies:photometry

1. Introduction

A cluster of galaxies is an experimental laboratory for studying the evolution of galaxies in a dense environment. It is difficult, in general, to study the evolution of galaxies in the field, because without knowing their precise redshifts, accurate absolute magnitudes are difficult to estimate. On the other hand, a difference in the apparent magnitudes of galaxies in a cluster directly reflects the difference in the absolute magnitudes of individual objects. Thus, a basic requirement in astronomy, i.e., to place the objects at the same distance, is fulfilled in the case of galaxy clusters. Clusters, therefore, provide the best opportunity for studying the evolution of galaxies at various redshifts.

Without a few exceptions, brighter early-type galaxies tend to have colors that are redder than their fainter counterparts, which is well known as a color–magnitude (CM) relation. The

same is true for galaxies in clusters; for example, the CM relations of elliptical and S0 galaxies in Virgo and Coma clusters are almost identical: scatters in colors along the CM relations are comparable to the observational photometric errors, suggesting virtually no scatters along the CM relations of the two clusters (Bower et al. 1992). The CM relations of ~ 40 nearby clusters are also very similar to those of the Virgo and Coma clusters (López-Cruz 1996). This strongly suggests that early-type galaxies, particularly ellipticals, formed and evolved very similarly in all clusters of galaxies.

The CM relation of elliptical galaxies has usually been interpreted as a stellar metallicity effect; mean stellar metallicities become progressively higher in brighter galaxies (Arimoto, Yoshii 1987). This conventional view of the CM relation, however, was challenged by Worthey (1996), he claimed that a stellar age effect should equivalently explain the observed CM relations if mean stellar ages become younger in fainter galaxies. Kodama and Arimoto (1997) calculated two evolutionary sequences of elliptical galaxies by assuming that the CM relation is caused either by a metallicity effect or by an age effect. They compared the theoretical CM relations with the empirical ones in the case of two clusters of galaxies, Abell 2390 at $z = 0.228$ and Abell 851 at $z = 0.407$. While the CM relations of the metallicity sequence at $z = 0.2$ and $z = 0.4$ almost perfectly match the empirical relations of Abell 2390 and Abell 851, respectively, those of the age sequence at $z = 0.2$ and $z = 0.4$ are too blue to be compatible, which led Kodama and Arimoto (1997) to reject the age effect as being the origin of the CM relation. Kodama et al. (1998) further extended a sample of distant clusters reaching $z \simeq 1.2$, to which they applied a model of passively evolving ellipticals (i.e., the metallicity sequence), and concluded that all of the CM relations of ellipticals in their sample clusters ($0.3 < z < 1.2$) are consistent with a picture of passively evolving ellipticals, and are explained only if they formed at $z_f > 2.5 - -4.5$.

However, a study of the CM relations is not sufficient to conclude that all ellipticals in clusters formed at such a high redshift, because late comers, such as recently formed ellipticals, presumably due to gas-rich spiral–spiral mergers, would quickly become red and locate at the bluer edge of the CM relation. Such young ellipticals could not be clearly separated from genuinely old ellipticals unless their colors are determined with photometric errors much smaller than the present day observations. If ellipticals had formed continuously since $z \gtrsim 2$, the luminosity function of ellipticals should show strong evolution since then. Although such indication seems to be detected for bright galaxies (Kauffmann, Charlot 1998; Aragón-Salamanca et al. 1998), other studies for clusters and field early-type galaxies showed that they followed passive evolution until $z \sim 1$ (De Propris et al. 1999; Kajisawa et al. 2000; Im et al. 2001).

Butcher and Oemler (1978) first pointed out that there is an excess of blue galaxies in high-redshift clusters compared with galaxy clusters at low redshift (Butcher–Oemler effect: Butcher, Oemler 1984; Margoniner, de Carvalho 2000). Later, by using spectroscopy and [O II] photometry, Dressler, Gunn (1982) claimed that the Butcher–Oemler effect already existed in clusters at distance of $z > 0.4$. The Butcher–Oemler effect has been extensively studied since then

(Newberry et al. 1988; Luppino et al. 1991; Dressler, Gunn 1992), and yet due to large observational and statistical uncertainties it is still difficult to quantify the phenomenon precisely, which prevents us from identifying the physical mechanisms that cause the effect. However, whatever the primary mechanism causing the blue excess is, it remains to be established whether it is still at work at the present time or, rather, appeared abruptly beyond $z \simeq 0.1$ (Molinari et al. 1994). Therefore, a systematic study of galaxy colors in nearby clusters is highly required.

X-ray satellites discovered hot intracluster medium (ICM) in clusters of galaxies (see Sarazin 1986). The ICM contains a significant amount of iron, which is certainly ejected from cluster galaxies. There is a good correlation between the amount of iron in the ICM and the total blue luminosity of cluster ellipticals and S0s, and the so-called iron mass-to-luminosity ratio (IMLR) is claimed to be universal in all clusters (Arnaud et al. 1992). The ASCA X-ray satellite greatly increased the number of clusters with the measured iron mass in the ICM. Nevertheless, the sample of clusters with known IMLR is as small as before ASCA, since the photometric data of many clusters which now have new iron abundance measurements by ASCA are not available. Therefore, it is still not clear if the IMLR is universal among clusters of galaxies. The answer is particularly important in studying the chemical enrichment history in clusters.

Thanks to a large field of view, the Schmidt Telescope is one of most suitable facilities for carrying out photometric observations of *nearby* clusters. The multicolor photometries give the SEDs of all objects in the field, from which, as we demonstrate in this work, the candidates of cluster galaxies can be selected. This article is the first of a series of Beijing–Arizona–Taipei–Connecticut (BATC) multi-color photometries of nearby clusters of galaxies. Our aim is to derive the luminosity functions and the CM relations for as many as possible cluster samples and to find descendants of the Butcher–Oemler galaxies at $z < 0.1$. This would also provide the total luminosities of cluster ellipticals and S0s, which would then be used for estimating the IMLRs of clusters.

This paper is organized as follows. In section 2, we show the observation. The data reduction and the flux calibration are described in sections 3 and 4, respectively. The catalog and error analysis are given in section 5. A method and result of member galaxy selection are shown in section 6. In section 7, we show color–color and color–magnitude diagrams to demonstrate the possibility of member galaxy selection by using the SEDs. We give our conclusions in section 8. The cosmological parameters $H_0 = 50$ km s^{-1} Mpc^{-1} and $q_0 = 0.5$ have been assumed.

2. Observations

Abell 566 (Zw 0658.3+6320) is a compact cluster of galaxies of BM type II-III (Bautz 1972). Redshifts were determined for central bright galaxies, ranging from $z = 0.095$ to 0.100 (Sargent 1973; Sarazin et al. 1982; Struble et al. 1987a, 1987b; Abell el al. 1989; Slinglendet al. 1998). The luminosity distance is 585 Mpc (Harris et al. 1982). The number of cluster galaxies is rather uncertain. Zwicky et al. (1968) counted 189 galaxies within a radius of 0◦.57. Abell et al. (1989) counted 127 galaxies that are not fainter than 2 mag from the third-brightest cluster member within the so-called Abell radius of $1.5h^{-1}$ Mpc, or $0^\circ.36$ (see also, Abell 1958; Corwin 1974).

The large field multi-color observations of Abell 566 were made with the BATC multicolor photometric system between 1995 March 18 and 2002 January 28. The instruments include the 60/90

cm f/3 Schmidt Telescope of National Astronomical Observatories (NAOC), located at the Xinglong station, altitude 900 m, about 150 km north-east from Beijing, China. A full description of the NAOC Schmidt, CCD and the data-acquisition system, and a definition of the BATC filter system are detailed elsewhere (Fan et al. 1996; Zhou et al. 2001).

A Ford 2048×2048 CCD camera was attached to the prime focus. The field of the image covers 0.95 deg^2 of sky with $1''.7$/pixel. Figure 1 shows the image of Abell 566 field converted from color images composed of the three images by U, h, and o filters. A U-band filter and 15 intermediate-band filters cover the whole optical wavelength range from $300nm$ to $1000nm$. Filter numbers, filter names, effective wavelength centers, and FWHMs of the sixteen filters are given in columns (1), (2), (3), and (4) of table 1, respectively. Figure 2 shows the latest measurement transmissions of the 15 BATC filters (see detail in Fan et al. 1996 and Zhou et al. 2003). There are only small differences in the transparency of filters between the new and previous measurements. In total, we made more than 85 hours of exposures on the Abell 566 to get 343 images in 16 colors. Columns (5) and (6) of table 1 give the exposure time (s) and the number of images, respectively.

Almost all nights were thought to be photometric by the observers. The standard stars were observed between air-masses 1 to 2 for each programmed filter band. Normally, 4 to 6 filters were selected to make flux calibration during each photometric night. The standard stars were put near the CCD center and only 300×300 pixels of sub-images were taken for the standard stars for saving readout time and disk space. The extinction coefficient and the magnitude of the zero point obtained from standard stars were used for making the flux calibration on BATC field images. The details of the observation for the calibration were described in Zhou et al. (2001).

3. Data Reduction

The bias subtraction and dome flat-field correction were done on the CCD images in the same way as we have done before named as PIPELINE I (Fan et al. 1996). The cosmic ray and bad pixel effect were corrected by comparing the images. The images were re-centered and position calibration was performed by using the Guide Star Catalog (GSC; Jenkner et al. 1990). By comparing hundreds bright stars in GSC, we could obtain 8 plate parameters and check the astrometry errors. The astrometry precision is about $0''.5$ for all of the images. The fluxes of intermediate-band filter images were calibrated by Oke–Gunn standard stars (Oke, Gunn 1983; Fukugita et al. 1996).

For both stars and galaxies, the magnitudes were measured with the aperture photometry and with a detection threshold of 4σ of the sky fluctuation per pixel. A minimum of 1 pixel above the threshold was required for detection. This might introduce a false detection, particularly near very bright stars and at the faint end magnitude. The sources detected in only 1 pixel are usually very faint and should suffer from rather large measurement errors. We considered the objects as being real only when the sources were detected in at least 3 different filter bands. Thus, most of objects in the final catalog should be real sources. All of these works of photometry were done by the PIPELINE II software, developed based on the basis of the DAOPHOT (Zhou et al. 2003). As a result of PIPELINE II procession, the magnitude of point-spead function (PSF) fitting and the magnitude of different aperture of 10751 objects were obtained. For measuring SEDs of the member galaxies in the cluster, we only used the aperture magnitude for this work.

The seeings were very different among the combined images of different filter bands, but typically $5''$. Since most galaxies in the images are obviously extended, they can not be regarded as point sources. We finally selected a fixed aperture of 5 pixels ($8''.5$) to do the photometry, which was large enough to make different seeing effects negligible. Although the photometry with fixed aperture gives no physical relation between the resulting magnitudes and the total magnitudes of galaxies, it should give reliable color indices (i.e., relative SEDs) of all the sources.

4. Flux Calibration

Four standard stars, BD+17°4708, BD+26°2606, HD19445, and HD84937 of Oke and Gunn (1983) were used for the BATC flux calibration. The absolute fluxes of these stars were taken from Fukugita et al. (1996). The definitions of the BATC magnitude are in the AB_ν system of Oke and Gunn (1983):

$$m_{\rm BATC} = -2.5 \cdot \log\widetilde{F_\nu} - 48.6. \quad (1)$$

Once aperture photometries on the image of standard stars are performed, the extinction coefficient, K, and magnitude zero point, C, can be obtained by fitting the extinction curve of magnitude versus airmass

$$m_{\rm instrument} - m_{\rm BATC} = K \cdot X + C \quad (2)$$

where X is the airmass of image. K and C are derived by a median fitting of the data points with straight line.

As supposed, the change of the instrumental zero point is very small within a short time (in scale of a few hours), the main variation in calibration with time is the variation of weather. We need a time- dependent term on K to trace the variation of the earth atmosphere. We used a smoothed continuous curve to trace the variation. Each fitted point is the mean value of all observing points within two hours. A higher weight is given to the nearby points in time, $1/[1.0 + (T_{\rm fit} - T_{\rm obs})^2]$, where $T_{\rm fit}$ and $T_{\rm obs}$ are the time of fitting and the observation point in units of hour, respectively.

A good trace of the extinction variation needs a set of good estimates of the mean extinction coefficient, K, and the instrumental zero point, C. While good estimates of K and C need information about the atmospheric variation. A few iterations are therefore required to determine K, C, and the variation. Fortunately, for almost all nights, the iteration converges quickly within 4 iterations, but for security, it is performed up to 10 times.

Once K and C were obtained, we could make a flux calibration in a traditional way (Zhou et al. 2003)

For our large field multicolor photometric system, we developed an alternative method to calibrate the SED of objects based on the fitting of the SED library to the observed multi-color photometry (Zhou et al. 1999; hereafter the model calibration). In this method, we suppose that most of the bright sources found in the image field are normal stars. No interstellar reddenings are assumed for both observed and library star SEDs (Gunn, Stryker 1983). In this case, for un-calibrated SEDs, each color needs a correction constant. We change iteratively the constant of each color until most of the sources can find their similar SEDs in the SED library. In the end, the corrected SEDs will be the same as the calibrated SEDs by the observation of standards. This method can improve

the quality of observations which are not taken under perfectly photometric conditions. The more passbands that are used for photometry, the better are the results. This technique has been applied to the BATC 15-passband CCD survey. By applying this method, the SED calibration was also done. A comparison was made between the results of this method and the normal magnitude calibration by using standard stars. Within a deviation due to galactic interstellar extinction, both methods gave the same results. The results of the model calibration were adopted in this paper as well as in our subsequent studies. Final catalog magnitudes were calibrated with the standard calibration results, and the SEDs were confirmed with the method of model calibration.

5. Catalogs and Error Analysis

A photometric SED catalog was obtained for all the sources ($\sim$10751) in the field of Abell 566. Since the size of the catalog is rather huge, we will distribute it electronically upon request. Table 2 gives the number of objects detected by each filter. The number of objects is relatively small in filters a and c, due to the short exposure times. We also give the magnitude limit, above which the catalog is complete for each filter. In these counts, a certain number of saturated objects are included, but these objects are explicitly excluded in the following data analysis.

Two kinds of error estimations have been checked. One was given by the photometric program of BATC PIPELINE II. The other was obtained by a comparison with the stellar spectral templates of Gunn and Stryker (1983).

The statistic errors given by the PIPELINE II are smaller than the real measurement errors. By comparing the errors obtained from different images of the same field in the same filter, we found that the measurement errors are typically $\pm$0.02 mag for bright objects. Statistical errors can be regarded as lower limits of the measurement errors. We fitted the magnitude error of objects in different magnitudes. In table 2, we give the limiting magnitude at the mean error of 0.1 for point sources. The estimated errors will be used to obtain threshold values for selecting the member galaxies of the cluster.

6. Photometric Redshift and Membership Determination

The photometric redshift technique was originally developed for detecting objects with high redshifts based on the broad-band photometries (Pelló et al. 1999; Bolzonella et al. 2000). Intermediate-band filters were used for photometries in the BATC survey, and the BATC SED for each object can be regarded as a rough spectrum. The advantages of the BATC data in measuring the photometric redshift of some faint galaxies can be expected. With the BATC SEDs (Yuan et al. 2001; Xia et al. 2002) and the combined SEDs by the BATC and SDSS observations (Yuan et al. 2003), the photometric redshifts of faint galaxies can be estimated with a certain accuracy ($\Delta z_{\rm phot} \approx 0.02$), which allows us to isolate the member galaxies for nearby galaxy clusters.

The technique involving the BATC photometric redshift was tested in our previous work (Xia et al. 2002). The mean estimate error of our photometric error is about 0.02–0.03. We adapted the Hyperz code (Bolzonella et al. 2000) to our 16-band photometric system. The redshifted spectral templates of normal galaxies were used to fit the observed SEDs, and the reddening law was set to be a free parameter during the fitting. The photometric redshift for each galaxy was searched in a

redshift range from 0.0 to 1.0, with a searching step of 0.01.

The histogram of $z_{\rm phot}$ for all galaxies is plotted in figure 3, which shows that most of them are located at $z < 0.3$. There are 11 central bright galaxies with known spectroscopic redshifts from NASA/IPEC Extragalactic Database (NED). By comparing the photometric redshift and the spectroscopic redshift, we found that our measurement error of redshift is about 0.008 (see also Xia et al. 2002). Considering measurement errors in photometry, we estimated the error of our photometric redshift to be about 0.03. From the shape of the histogram profile of redshift distribution, we estimated that the member galaxies of Abell 566 should have photometric redshifts within the range $[0.05, 0.15]$; thus we took this range as the criteria for membership selection. As a result, 561 galaxies were selected as candidates. The candidates include 45 of 54 extra-galaxies known in NED. It also includes 60 of 95 sources showing an extended morphology in our images. It should be noted that the uncertainty of the photometric redshift is rather large compared to the intrinsic dispersion of the galaxy cluster, but it can still be used to select the member galaxies with high efficiency.

We found that many of the observed SEDs of galaxies are very similar to the template spectra. As an example, figure 4 shows a comparison between the observed SED of a galaxy at the cluster center and a template spectrum. The galaxy is located at $(\alpha_{2000}, \delta_{2000}) = (07^h04^m28^s.86, 63^\circ18'38''.0)$. In the upper panel, the asterisks with error bars define the observed SED and the line gives the best fit SED of galaxy template given by Hyperz. In the lower panel, the horizontal bars indicate the observed flux of this galaxy, onto which the spectrum of a template S0 galaxy (Kinney et al. 1996) shifted to $z = 0.1$ is superposed. The spectroscopic redshift of the galaxy is $z_{\rm spec} = 0.0973$, while our photometric estimate gives $z_{\rm phot} = 0.091$. The result of a comparison shows a very good quality of the SED fitting, which demonstrates a potential possibility of the member galaxy detection. In a similar way, 10 other galaxies with spectroscopic redshift are shown in figure 5.

7. Some Tests on the Catalog

The color–color and the CM diagrams are usually used for studying statistically the characteristics of objects in a cluster of galaxies. They are indeed useful tools to separate the different kind of objects as well as to make a comparison with theoretical models. We have the SEDs with 16 filter bands, of which specially selected colors can be used for studying the stellar populations of cluster galaxies in the Abell 566.

As an initial test, here we show two color–color diagrams. One is a mag(370 nm) - mag(607 nm) versus mag(607 nm) - mag(919 nm) color–color diagram. The other is the mag(370 nm) - mag(492 nm) versus mag(607 nm) - mag(919nm) diagram. These diagrams are shown in figure 6 and figure 7, respectively, in which we also plot the distribution of template stars (Gunn,Stryker 1983). We can find in these diagrams that almost all of the galaxies selected by their SED of 16 bands are located above the field stars. There is a clear gap between the galaxies and the stars, especially in the red part of the galaxy sequence. We use two lines to mark the area occupied by the cluster galaxies. These diagrams show the possibility of selecting the member galaxies from their SED properties (photometric redshift).

A CM diagram is shown in figure 8. A sequence of early-type candidate galaxies is clearly seen as a red envelope of the cluster galaxies. Together with other CM diagrams, it will be used later

to study the evolution of galaxies in the cluster with the help of an evolutionary synthesis model of Kodama (1997) and Kodama and Arimoto (1997).

We try to cull early-type galaxies basing on mag (421 nm)-mag (607 nm) in figure 8. We tentatively regard galaxies of mag (421 nm) - mag(607 nm) > 1.4 as early-type (or red) galaxies and other galaxies as late-type (blue) galaxies. We show the radial distribution of red and blue galaxies in figure 9. We find that, compared with blue galaxies, the number density of red galaxies is much higher in the cluster central region, while lower in the outer part of the cluster. Finally, we show the distribution of all all the cluster member candidates in the field of view and its density contour map in figure 10.

The distribution of different galaxies in the cluster may reflect a galaxy– environment relation. That means that an environmental factor plays an important role in determining the morphology of a galaxy (Hubble, Humason 1931). Oemler (1974) gave the first quantitative evidence that the morphological types vary within individual clusters. His morphology– radius relation shows that the projected density of spiral galaxies actually increases with radius in the inner part of a cluster. Similarly, Melnick and Sargent (1977) found that the S0s become increasingly dominant at small radii. Dressler (1980) showed that the morphology of galaxies in 6 cluster varies as functions of the radius and the local projected galaxy density. He argued that a fundamental relation is the density–morphology relation, which has been further studied by Merrifield and Kent (1989) and Whitmore, Gilmore, and Jones (1993). Our results are consistent with these previous studies.

The observational results presented in this work – membership and the SEDs – will be used for studying the cluster properties of Abell 566. In our subsequent paper, we will work on the age and metallicity of galaxies, possible Butcher–Oemler effect at $z \simeq 0.1$, and the IMLR, with which we will be able to give a detailed insight on evolution of cluster galaxies in the local universe.

8. Conclusions

During several years of runs of the BATC survey (1995–2002), more than 86 hours of exposures on the field of Abell 566, a cluster of galaxy at redshift $z \simeq 0.1$, were accumulated, which included 343 2k $\times$ 2k images in 15 intermediate-band filters and the wide band U-filter. With the magnitude limit of $V \sim 20$ mag, more than 10751 objects were detected in the common area in at least 3 filter band images. By a fixed aperture photometric measurement, we obtained the SEDs of all the detected objects that cover the wavelength from 300 nm to 1000 nm. By a method involving the photometric redshift, 561 objects were selected as candidates of the cluster member galaxy. We analyzed the magnitude measurement errors, and gave an SED catalog of the selected galaxies. Base on the color–color and color–magnitude diagrams, we show the possibility of SED selection of cluster member galaxies. We show the distribution of the galaxies in the cluster. We use red and blue galaxies to represent the early-type and late-type galaxies, respectively. From the distribution of the two kind of member galaxies, we find that the early-type galaxies have a much higher density than late-type galaxies in the central region of the cluster, while the number density of the late-type galaxies are higher in the outer part of the cluster. The results of this work will be used to study the evolution of galaxy populations in the cluster Abell 566 in our subsequent paper.

———————-

The work is partly supported by the National Sciences Foundation of China (NSFC) and the National Key Basic Research Science Foundation (NKBRSF TG199075402) and a Grant-in-Aid for Scientific Research (No.116402307) by the Japanese Ministry of Education, Culture, Sports, Science and Technology. X. Zhou would like to thank Masaru Matsuoka and Nobuyuki Kawai who helped in his stay at RIKEN (Japan) where most of this article was prepared. We also thank Yao-Hua Li, Hong Wu, Jin Zhu, and Suijian Xue for his management and support of the instruments, Ray Chen, Hao-tong Zhang, Bing Zhao, and Zheng Zheng, who obtained many of the observations for the BATC and shared their experience with us. We also thank the assistants who helped with the observations for their hard work and kind cooperation.

References

Abell, G.O. 1958, ApJS, 3, 211

Abell, G.O., Corwin, H.G.,Jr. & Olowin, R. P. 1989, ApJS, 70, 1

Aragón-Salamanca, A., Baugh, C. M., & Kauffmann, G. 1998, MNRAS, 297, 427

Arimoto, N., & Yoshii, Y. 1987, A&A, 173, 23

Arnaud, M., Rothenflug, R., Boulade, O., Vigraux,L., & Vangioni-Flam,E. 1992, A&A, 254, 49

Bautz, L.P. 1972, AJ, 77, 1

Bolzonella, M., Miralles, J.-M., & Pelló, R. 2000, A&A, 363, 476

Bower, R.G., Lucey, J.R., & Ellis, R.S. 1992, MNRAS, 254, 601

Butcher, H., & Oemler, A.,Jr. 1978, ApJ, 219,18

Butcher, H., & Oemler, A.,Jr. 1984, ApJ, 285,426

Corwin, H.G.,Jr. 1974, AJ, 79, 1356

De Propris, R. Stanford, S.A., Eisenhardt, P.R., Dickinson,M., & Elston,R. 1999, AJ, 118 719

Dressler, A. 1980, ApJ, 236, 351

Dressler, A., & Gunn, J.E. 1982, ApJ, 263, 533

Dressler, A., & Gunn, J.E. 1992, ApJS, 78, 1

Fan, X. et al. 1996, AJ, 112, 628

Fukugita, M., Ichikawa,T.,Gunn,J.E.,Doi,M., Shimasaku,K., & Schneider,D.P. 1996, AJ, 111, 1748

Gunn, J.E., & Stryker, L.L. 1983, ApJS, 52, 121

Harris, D.E., Robertson, J.G., Dewdney, P.E., & Costain,C.H. 1982, A&A, 111,299

Hubble, E.P., & Humason, M.L., 1931, ApJ, 74, 31

Im, M., Faber,S.M., Gebhardt,K., Koo,D.C., Phillips,A.C., Shiaron,R.P., Simard,L.,Willmer,C.N.A. 2001, AJ, 122, 750

Jenkner, H., Lasker, B. M., Sturch, C. R., McLean,B.J., Shara,M.M., & Russell J.L. 1990, AJ, 99, 2082

Kajisawa, M., et al. 2000, PASJ, 52, 53

Kauffmann, G., & Charlot, S. 1998, MNRAS, 297, L23

Kinney, A.L., Calzetti,D., Bohlin,R.C., McQuade,K., Storchi-Bergmann,T., Schmott,H.R. 1996, ApJ, 467, 38

Kodama, T. 1997, PhD Thesis, The University of Tokyo

Kodama, T., & Arimoto, N. 1997, A&A, 320, 41

Kodama, T., Arimoto, N., Barger, A.J., & Aragón-Salamanca, A. 1998, A&A, 334, 99
López-Cruz, O. 1996, PhD Thesis, University of Tronto
Luppino, G.A., Cooke, B.A., McHardy, I.M., & Ricker, G.R. 1991, AJ, 102, 1
Margoniner,V.E., & De Carvalho,R.R., 2000, ApJ, 119, 1562
Melnick,J., & Sargent,W.L.W. 1977, ApJS, 215, 401
Merrifield, M.R., & Kent,S.M., 1989, AJ, 98, 351
Molinari, E., Banzi, M., Buzzoni, A., Chincarini, G., & Pedrana, M.D, 1994, A&AS, 103, 245
Newberry, M.V., Kirshner, R.P., & Boroson, T.A. 1988, ApJ, 335, 629
Oemler, A. 1974,ApJ, 194, 1
Oke, J. B., & Gunn, J. E. 1983, ApJ, 266, 713
Pelló, R., et al. 1999, A&A, 346, 359
Sarazin, C.L., Rood, H.J., & Struble, M.F. 1982, A&A, 108, L7
Sarazin, C.L. 1986, Rev. Mod. Phys., 58, 1
Sargent, W.L.W. 1973, PASP, 85, 281
Slinglend, K., Batuski, D., Miller, C., Haase,S., Michaud,K., & Hill, J.M. 1998, ApJS, 115, 1
Struble, M.F., & Rood H.J. 1987a, ApJS, 63, 543
Struble, M.F., & Rood H.J. 1987b, ApJS, 63, 555
Whitmore, B.C., Gilmore, D.M., & Jones, C. 1993, ApJ, 407, 489
Worthey, G., Trager, S.C., & Faber, S.M. 1996, in Fresh Views of Elliptical Galaxies, ed. A.Buzzoni, A.Renzini, & A.Serrano (SanFrancisco: ASP), 203
Xia, L. et al. 2002, PASP, 114, 1349
Yuan,Q. et al. 2003, ApJaccepted
Yuan, Q., Zhou, X., Chen, J., Jiang, Z., Ma, J., Wu, H., Xue, S., Zheng,Z., & Zhu, J. 2001, AJ, 122, 1718
Zhou, X., et al., 2003, A&A, 397, 361
Zhou, X., Chen, J.S., Xu, W., Zhang, M., Jiang, Z.J. & Zhu, J. 1999, PASP, 111, 909
Zhou, X., Jiang, Zh. J., Xue, S. J., Wu, H., Ma, J., Chen, J. S.,2001, ChJAA, 1, 372
Zwicky, F., et al. 1968, Catalogue of Galaxies and Clusters of Galaxies, (Pasadena:CIT)

Table 1. Parameters of the BATC filters and the statistics of the observation.

No	Name	λ (nm)	FWHM (nm)	Exp-Time(s)	Images	Calib.	Calib-err.
0	U	370	70.0	41400	15	5	0.013
1	a	330	35.9	3600	3	1	0.055
2	b	389	29.1	17400	25	5	0.012
3	c	421	30.9	10200	12	4	0.013
4	d	455	33.2	36600	43	6	0.011
5	e	492	37.4	18600	29	5	0.007
6	f	527	34.4	24000	34	12	0.004
7	g	579	28.9	31200	39	11	0.003
8	h	607	30.8	18300	23	9	0.004
9	i	666	49.1	18000	24	11	0.004
10	j	705	23.8	18600	26	11	0.003
11	k	749	19.2	16800	22	7	0.003
12	m	802	25.5	16800	14	4	0.004
13	n	848	16.7	36000	30	2	0.011
14	o	919	24.7	10920	10	2	0.034
15	p	974	27.5	20400	18	2	0.055

Table 2. Number of detected sources and magnitude at mean magnitude error of 0.1 for point sources

BATC filter	Number of sources detected	Mag limit
U	9289	21.1
a	7851	18.8
b	8162	18.9
c	9209	20.1
d	9388	19.9
e	9837	19.8
f	9776	19.8
g	10092	19.8
h	10040	19.9
i	10056	20.2
j	10219	19.1
k	10449	19.2
m	9722	18.5
n	9951	18.4
o	9976	17.8
p	9617	17.4

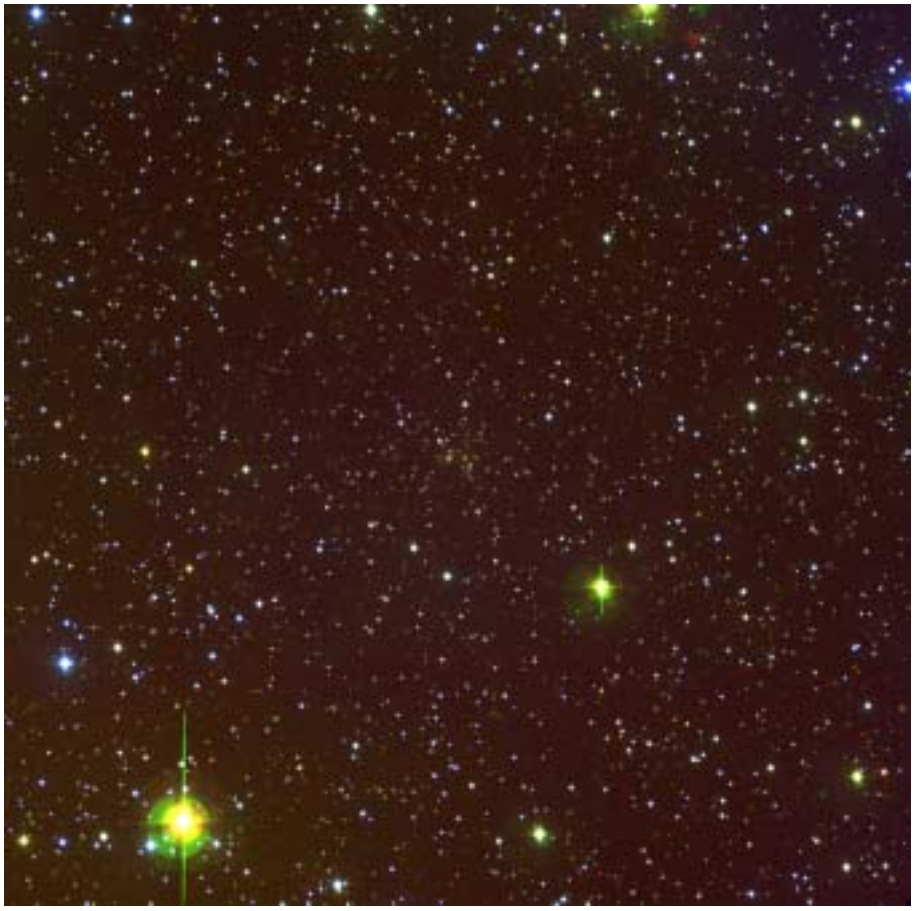

Fig. 1. Image of the Abell 566 field converted from color images with filters U, h, and o. The size of the field is about $58' \times 58'$.

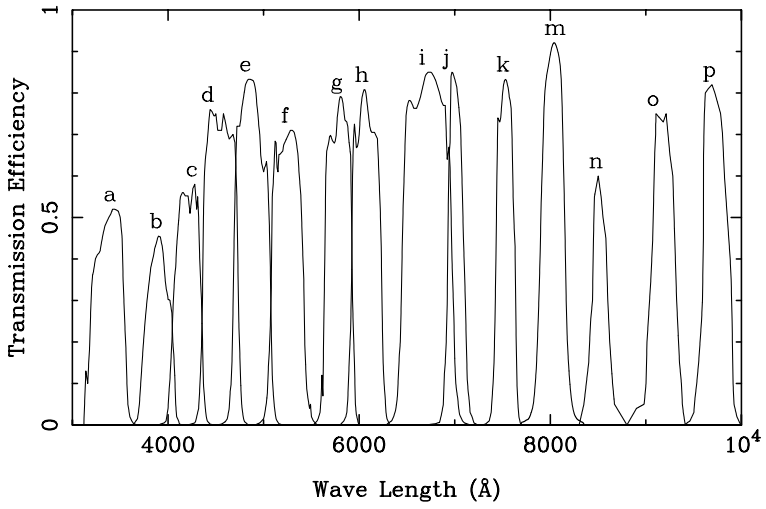

Fig. 2. Transmissions of the 15 BATC filters. The filter codes (see table 1) are labeled on the top of each filter.

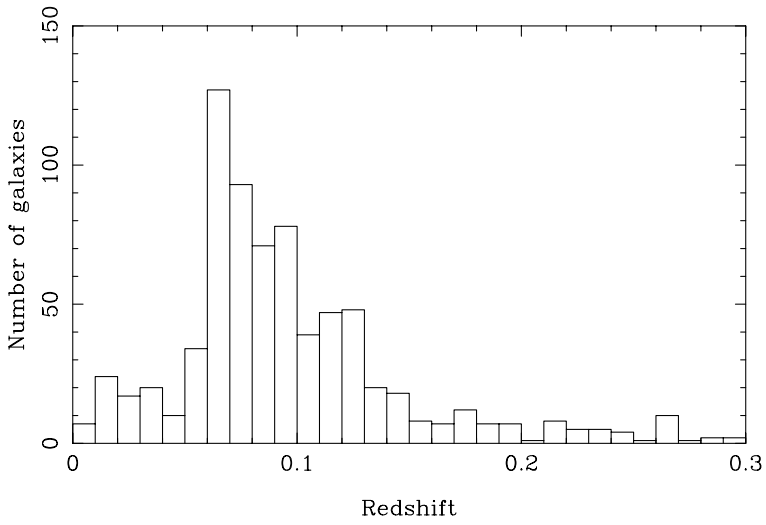

Fig. 3. Histogram of $z_{\rm phot}$ for all galaxies.

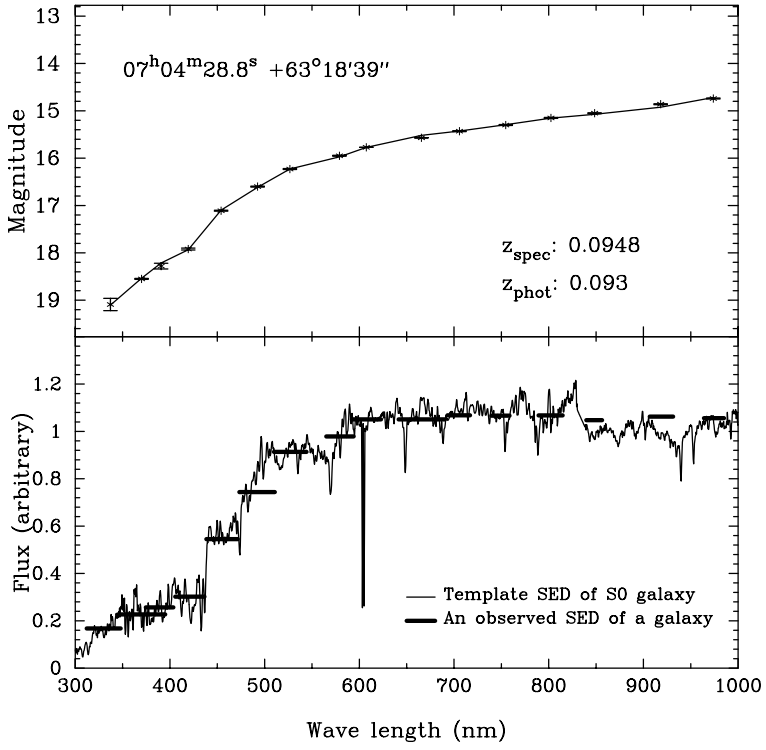

Fig. 4. Upper panel: Observed magnitudes of a galaxy located at $(\alpha_{2000}, \delta_{2000}) = (07^h04^m28^s.86, 63°18'39'')$ (asterisks) and the best fit SED of galaxy template (thin line). Lower panel: Observed energy fluxes of the same galaxy (bars) onto which a spectrum of an S0 galaxy at $z = 0.1$ is superposed (Kinney 1996).

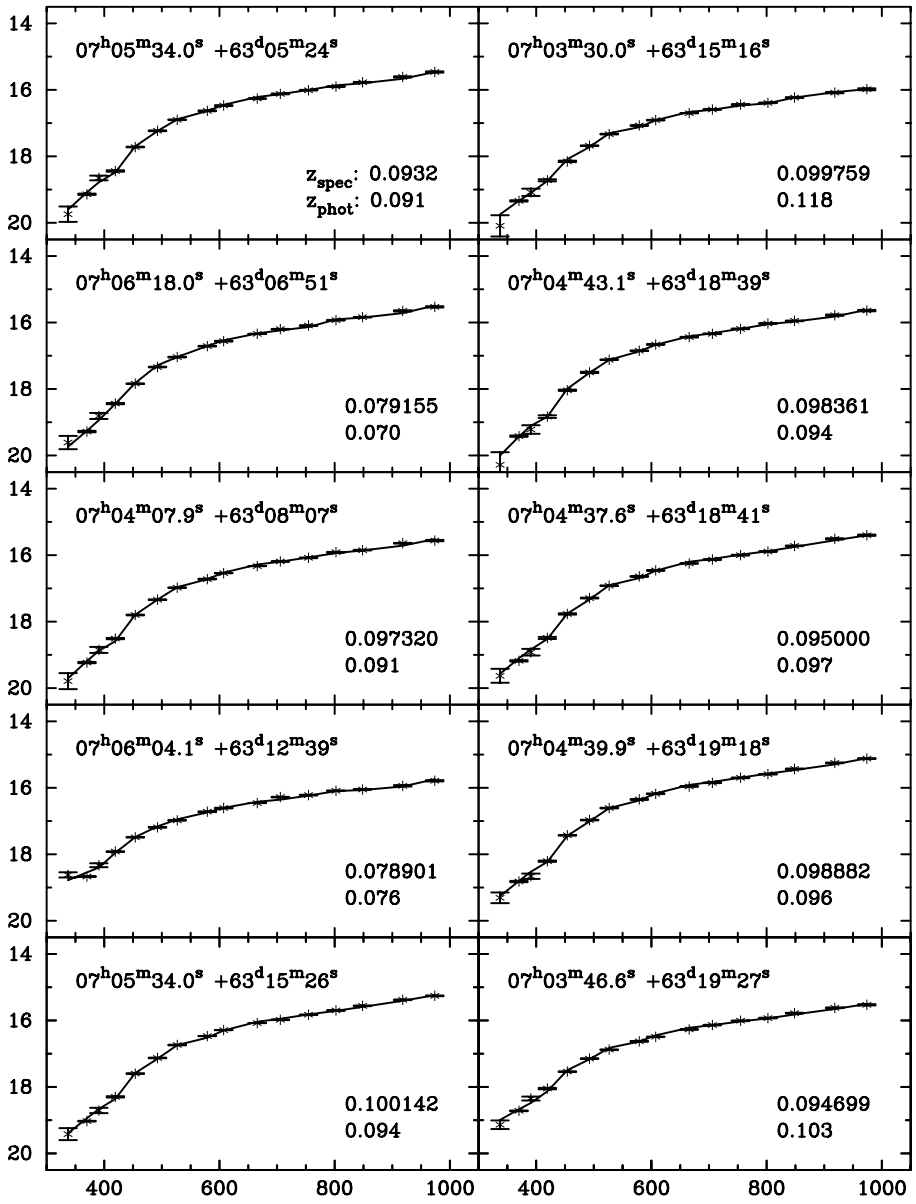

Fig. 5. Same as the upper panel of figure.4, but for 10 other galaxies with known spectral redshifts.

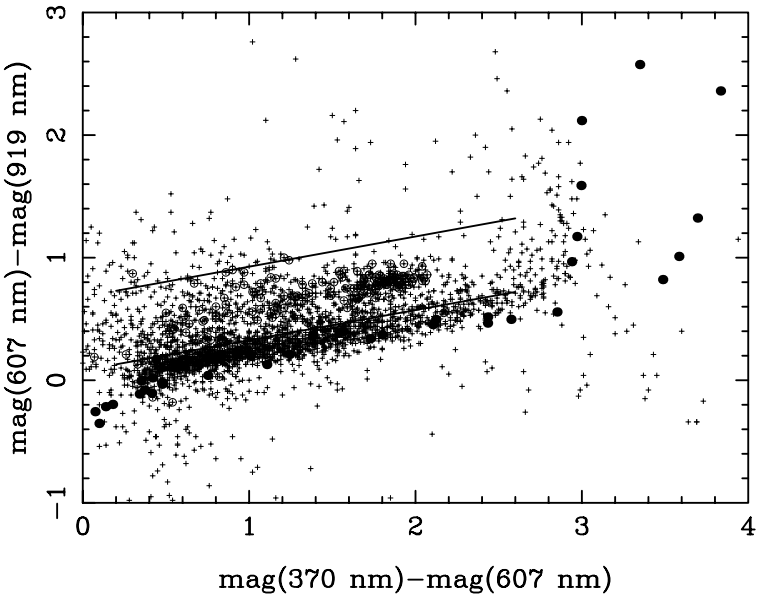

Fig. 6. mag (370nm) − mag (607nm) versus mag (607nm) − mag (919nm) color–color diagram. Circled crosses indicate galaxies selected according to morphological shapes. The small crosses are the field stars. The filled circles give the template stars of different type. The two solid lines mark the area occupied by the cluster galaxies.

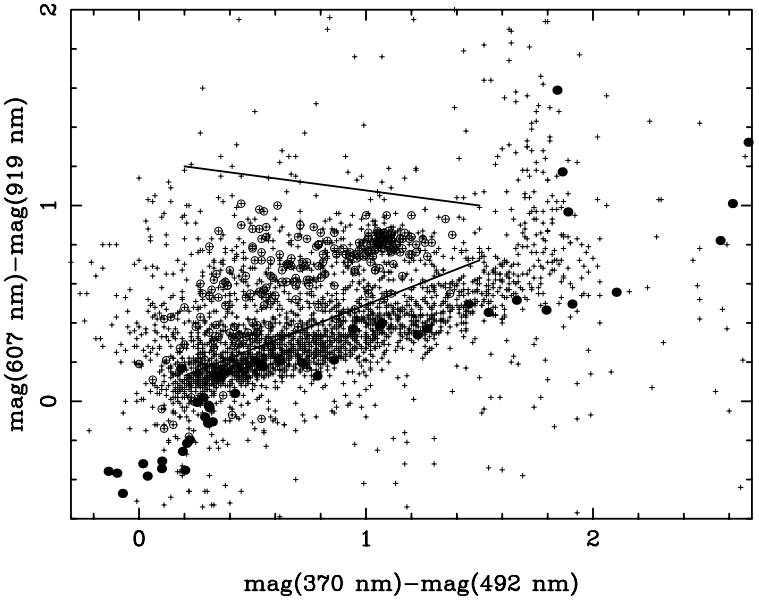

Fig. 7. Same as figur.6, but for the mag(370 nm) − mag (492 nm) versus mag (607 nm) − mag (919 nm) diagram.

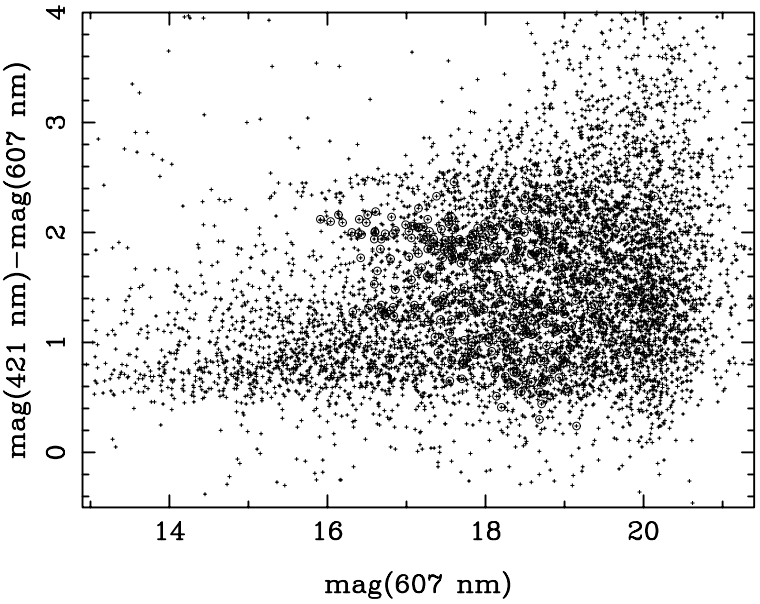

Fig. 8. mag (607 nm) versus the mag (421 nm) − mag (607 nm) color–magnitude diagram. Symbols are the same as in figur.6.

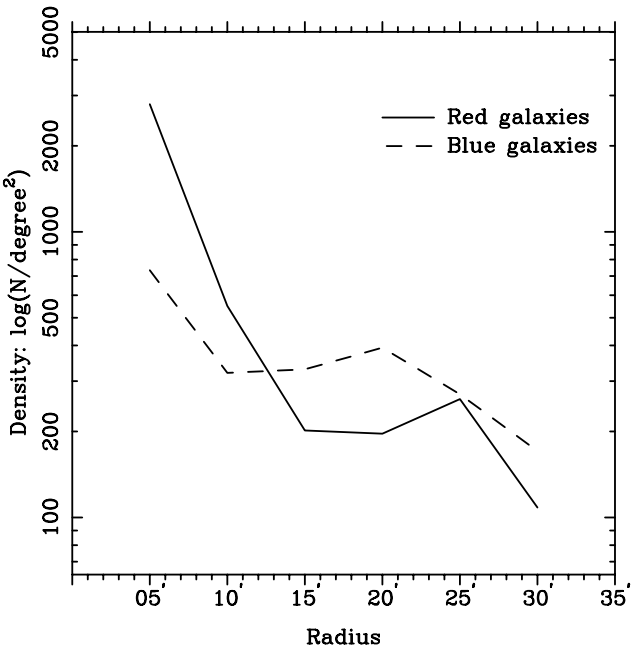

Fig. 9. Distribution of the number density of red and blue galaxies, which represent early-type and late-type galaxies, respectively.

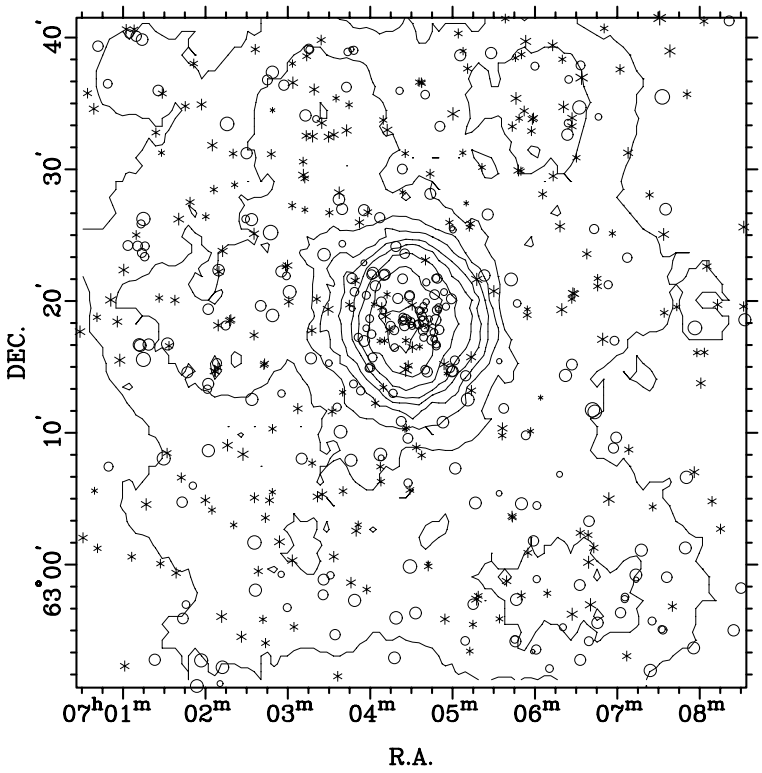

Fig. 10. Contour map of all member galaxy candidates of Abell 566 chosen by the method of photometric redshift. The position of the red galaxies are presented as circles and the blue galaxies are shown in star sign. The contour map is in interval of 10 galaxies per square degree.